

Article

Optimized Trajectory Tracking for Robot Manipulators with Uncertain Dynamics: A Composite Position Predictive Control Approach

Shanrong Ren ¹, Linyan Han ² , Jianliang Mao ³  and Jun Li ^{1,*} 

¹ Ministry of Education Key Laboratory of Measurement and Control of Complex Systems of Engineering, School of Automation, Southeast University, Nanjing 210096, China; jackyren@seu.edu.cn

² School of Mechanical Engineering, University of Leeds, Leeds LS2 9JT, UK; l.y.han@leeds.ac.uk

³ College of Automation Engineering, Shanghai University of Electric Power, Shanghai 200090, China; jl_mao@shiep.edu.cn

* Correspondence: j.li@seu.edu.cn

Abstract: This study addresses the trajectory tracking control challenges of robot manipulators with uncertain dynamics. The aim is to achieve precise and smooth trajectory regulation through a novel composite position predictive control (PPC) scheme that integrates motion profile and disturbance preview techniques. First, we perform offline dynamics identification and feedforward compensation alongside a pre-defined motion profile. To handle the disturbances arising from uncertain dynamics, a super-twisting disturbance observer is designed, resulting in a dynamically compensated prediction model. Furthermore, the receding optimization operations for PPC are executed by solving an optimal solution associated with a joint angle tracking error. The combination of feedforward and feedback control improves the robot manipulator's absolute positioning accuracy as opposed to the conventional model predictive control method, especially when dealing with uncertain dynamics. The effectiveness of the proposed control method is confirmed through trajectory tracking experiments conducted on a six-degree-of-freedom robot platform with varying end-effector loads. The experimental results demonstrate that the proposed PPC method enhances tracking accuracy by approximately 45% and 25% when compared to the traditional inverse dynamic control (IDC) and the robust IDC approaches, respectively.



Citation: Ren, S.; Han, L.; Mao, J.; Li, J. Optimized Trajectory Tracking for Robot Manipulators with Uncertain Dynamics: A Composite Position Predictive Control Approach. *Electronics* **2023**, *12*, 4548. <https://doi.org/10.3390/electronics12214548>

Academic Editor: Maciej

Ławryńczuk

Received: 30 September 2023

Revised: 29 October 2023

Accepted: 2 November 2023

Published: 6 November 2023



Copyright: © 2023 by the authors. Licensee MDPI, Basel, Switzerland. This article is an open access article distributed under the terms and conditions of the Creative Commons Attribution (CC BY) license (<https://creativecommons.org/licenses/by/4.0/>).

1. Introduction

Robot manipulators, typically consisting of interconnected motion chains and various joints, find widespread applications in high-end fields such as intelligent manufacturing [1,2], aerospace assembly [3,4], and medical surgery [5]. These applications often require robot manipulators to perform precise and efficient engineering tasks, leading to increased demands for high-precision trajectory tracking. However, in actual industrial scenarios, the prevailing control method still relies on cascade PID control, which is used to handle diverse complex operating conditions [6]. Nevertheless, robot manipulator systems are inherently nonlinear control objects with strong coupling and complex uncertainties. Relying solely on PID control, while it is commonly used, may not be sufficient to achieve the desired level of performance, especially in challenging industrial scenarios. The limitations of PID control in handling nonlinearities and uncertainties can lead to suboptimal trajectory tracking and potentially pose safety risks, making it essential to explore alternative control strategies [7].

As a result, there is a growing emphasis on researching advanced control algorithms for robot manipulators in complex environments, encompassing sliding mode control [8,9],

model predictive control (MPC) [10,11], adaptive control [12], and neural network control [13,14], among others. These control strategies aim to address the inherent challenges posed by nonlinear dynamics and uncertainties, providing potential solutions to enhance trajectory tracking accuracy, improve real-time capabilities, and ensure robust performance in unpredictable operating conditions. Among these approaches, MPC has emerged as a promising method due to its conceptual simplicity and excellent trajectory tracking performance, garnering significant attention from engineering practitioners [15]. In general, MPC strategies can be further classified into discrete-time optimization control and continuous-time optimization control [16]. The former is widely used to address internal state constraints for system optimization. However, it is important to consider that its control performance is significantly influenced by the sampling control period, and prioritizing control performance alone may result in an excessive computational burden, potentially affecting real-time capability [17]. In contrast, continuous-time predictive control circumvents the need for model discretization and directly utilizes the Taylor approximation of the system dynamics model to compute optimization performance indicators. This approach yields explicit analytical solutions, offering advantages such as simplicity in design, reduced computational load, and a clear parameter-tuning mechanism [18,19]. By advancing research on the continuous-time MPC, we can further enhance the effectiveness and efficiency of robot manipulators in challenging environments, benefiting various applications in industrial automation, medical robotics, and autonomous systems.

However, uncertainties, including parameter perturbations, unmodeled dynamics, and external disturbances, are pervasive in engineering systems and can significantly impact control performance and even lead to safety issues [20–22]. Achieving high-precision trajectory tracking control for robot manipulator systems in the presence of uncertainties poses a considerable challenge. Similarly, traditional MPC designs also face significant hurdles in handling uncertainties [23]. As an alternative, a common approach to tackle uncertainties is to utilize disturbance/uncertainty estimation attenuation (DUEA) techniques [24], which typically combine feedforward compensation and feedback control, providing enhanced trajectory tracking control for robot manipulators operating in uncertain environments. By mitigating the impact of uncertainties, DUEA techniques play a vital role in improving trajectory tracking accuracy and overall system robustness. For instance, as a popular DUEA technique, super-twisting-disturbance-observer (STDO)-based composite controllers have been successfully applied to many fields, such as underwater vehicles [25] and overhead crane systems [26]. Furthermore, several extensions for the STDO can also be found in the community of DUEA, such as the adaptive fast STDO [27] and the fixed-time STDO [28]. Moreover, it has also been reported that integrating DUEA techniques into the MPC design offers a promising solution for effectively addressing uncertainties and disturbances, ultimately enhancing the reliability of control operations in practical applications [29–31].

Based on the above analysis and inspired by reference [18], this paper investigates a composite position predictive control (PPC) approach for the trajectory tracking of robot manipulators. The proposed PPC scheme integrates motion profile and disturbance preview techniques to effectively address the uncertainties present in the system. Firstly, offline dynamics identification and feedforward compensation are performed in conjunction with a pre-defined motion profile. Additionally, a STDO is designed to handle the disturbances arising from uncertain dynamics, resulting in a dynamically compensated prediction model. Furthermore, the study executes receding optimization operations for the PPC by solving an optimal solution associated with a joint angle tracking error. This approach ensures optimal trajectory tracking performance, even in the presence of uncertainties. The effectiveness of the proposed control method is rigorously validated through various trajectory tracking experiments conducted on a six-degree-of-freedom (DOF) robot platform. The experimental results demonstrate superior trajectory control accuracy and disturbance rejection ability compared to the traditional inverse dynamic control (IDC) approach. Compared to existing research results, this paper's contributions are mainly reflected in the following two aspects:

- The combination of feedforward and feedback control improves the limitations of the traditional MPC in trajectory tracking accuracy under uncertain dynamics, thereby enhancing the robot manipulator's absolute positioning accuracy during operation.
- The proposed composite generalized predictive control scheme is experimentally validated using the Beckhoff motion controller and the actual robot system using the model-based design approach using MATLAB/Simulink.

The structure of this paper is as follows. Section 2 introduces the system dynamics and outlines the control objectives for robot manipulators. Section 3 presents a comprehensive design procedure, encompassing offline dynamics identification, uncertain dynamics estimation, and composite position predictive control design. Additionally, the stability analysis is also provided. In Section 4, we evaluate the performance of the proposed approach through real-world experimentation with a six-axis robot manipulator. Finally, Section 5 presents the conclusions.

Notations:

- $\mathbf{x} = [x_1, x_2, \dots, x_n]^\top$ denotes an n -dimensional vector, where x_i represents the i -th component of \mathbf{x} with $i = 1, 2, \dots, n$.
- $\mathbf{x}^a = [x_1^a, x_2^a, \dots, x_n^a]^\top$ with $0 < a < 1$; $\mathbf{x}^{(a)} = [x_1^{(a)}, x_2^{(a)}, \dots, x_n^{(a)}]^\top$ with $a \in \mathbb{N}^+$.
- $\text{sig}^a(\mathbf{x}) = [|x_1|^a \text{sign}(x_1), |x_2|^a \text{sign}(x_2), \dots, |x_n|^a \text{sign}(x_n)]^\top$ with $0 < a < 1$.

2. Problem Formulation

2.1. System Dynamics Modeling

For an n -link robot manipulator system, its dynamic model can be described in the following form [32]:

$$\mathbf{M}(\mathbf{q})\ddot{\mathbf{q}} + \mathbf{C}(\mathbf{q}, \dot{\mathbf{q}})\dot{\mathbf{q}} + \mathbf{G}(\mathbf{q}) + \mathbf{f}(\dot{\mathbf{q}}) = \boldsymbol{\tau} + \boldsymbol{\tau}_d \quad (1)$$

where $\mathbf{q}, \dot{\mathbf{q}}, \ddot{\mathbf{q}} \in \mathbb{R}^n$ are the vectors representing joint angles, angular velocities, and accelerations, respectively; $\mathbf{M}(\mathbf{q}) = \mathbf{M}^\top(\mathbf{q}) \in \mathbb{R}^{n \times n}$ is the mass and inertia matrix, which is symmetric and positive definite; $\mathbf{C}(\mathbf{q}, \dot{\mathbf{q}}) \in \mathbb{R}^{n \times n}$ is the Coriolis and centripetal forces matrix; $\mathbf{G}(\mathbf{q}) \in \mathbb{R}^n$ represents the gravitational term of the robot manipulator; $\mathbf{f}(\dot{\mathbf{q}}) \in \mathbb{R}^n$ represents the friction torque consisting of Coulomb and viscous friction; $\boldsymbol{\tau} \in \mathbb{R}^n$ is the joint torque generated by servo drives; and $\boldsymbol{\tau}_d \in \mathbb{R}^n$ accounts for the lumped disturbances, including parameterized uncertainties, unmodeled dynamics, and external uncertain load.

By defining the system states $\mathbf{q} = \mathbf{x}_1$ and $\dot{\mathbf{q}} = \mathbf{x}_2$, system (1) can be reformulated into the state-space representation as

$$\begin{cases} \dot{\mathbf{x}}_1 = \mathbf{x}_2 \\ \dot{\mathbf{x}}_2 = \mathbf{u} + \mathbf{F}(\mathbf{x}_1, \mathbf{x}_2) + \mathbf{d}(t) \\ \mathbf{y} = \mathbf{x}_1 \end{cases} \quad (2)$$

where

$$\begin{aligned} \mathbf{u} &= \mathbf{M}^{-1}(\mathbf{x}_1)\boldsymbol{\tau}, \mathbf{d}(t) = \mathbf{M}^{-1}(\mathbf{x}_1)\boldsymbol{\tau}_d, \\ \mathbf{F}(\mathbf{x}_1, \mathbf{x}_2) &= -\mathbf{M}^{-1}(\mathbf{x}_1)[\mathbf{C}(\mathbf{x}_1, \mathbf{x}_2)\mathbf{x}_2 + \mathbf{G}(\mathbf{x}_1) + \mathbf{f}(\mathbf{x}_2)]. \end{aligned} \quad (3)$$

Taking into account the actual attributes of system disturbances and the intended trajectory within practical industrial applications, we establish the following two assumptions concerning system (2):

Assumption 1. Both $\mathbf{d}(t)$ and its derivative term $\dot{\mathbf{d}}(t)$ are bounded, i.e., $\sup\{|d_i|, |\dot{d}_i|\} \leq L_i$, $i = 1, 2, \dots, n$, where $\mathbf{L} = \text{diag}(L_1, L_2, \dots, L_n)$ is a positive constant matrix.

Remark 1. In general, the external disturbances experienced by robotic systems can be quite intricate. These disturbances may originate from both human actions and the external environment, such as when unknown load disturbances occur. To evaluate the disturbance rejection capabilities,

we subject the robot's end-effector to the unknown load disturbance, as clarified in Section 4.3. In this context, the load disturbance can be treated as a constant, which is a practical engineering assumption. Then, it can be ascertained that the disturbance imposed at the joint remains continuously differentiable through Jacobian matrix mapping. Therefore, Assumption 1 can be considered reasonable.

Assumption 2. The trajectory planning for the robot manipulator in joint space is pre-established, i.e., the desired trajectory q_d , along with its corresponding velocity \dot{q}_d and acceleration \ddot{q}_d , are all known and exhibit continuity.

2.2. Control Objective

Generally, the control objective of a robot manipulator's trajectory tracking can be summarized as the following two aspects:

- **High Trajectory Tracking Accuracy:** This objective involves regulating the joint motion of the robot manipulator to attain the precise tracking of a predefined trajectory. The control system is required to ensure that the robot's end-effector accurately follows the intended trajectory while minimizing deviations.
- **Robustness to Uncertain Dynamics and Disturbances:** The control algorithm must be meticulously designed to accommodate fluctuations in the robot's dynamics, encompassing variations in joint friction, inertial parameters, and mechanical uncertainties. Additionally, the control system should effectively counteract external disturbances that may arise during operation, such as forces applied to the end-effector or unexpected environmental conditions.

By fulfilling the above control objectives, the robot manipulator can fluidly follow predefined trajectories with exceptional accuracy, all the while upholding resilience against uncertainties and disturbances. This achievement will enhance control precision, thereby securing the dependable performance of the robot manipulator across diverse operational scenarios.

3. Controller Design

Based on the aforementioned control objectives, this section provides an in-depth exposition of the proposed control strategy. The framework is primarily delineated by three fundamental constituents: offline dynamics identification, uncertain dynamics estimation, and composite predictive control design.

3.1. Offline Dynamics Identification

The objective of this subsection is to perform the offline identification of the system dynamics, which involves obtaining a mathematical description of the system through experimental data. Subsequently, feedforward compensation techniques are employed to introduce pre-computed compensatory signals into the controller, mitigating the influence of system dynamics on control performance.

To begin with, leveraging the attributes of friction, we select a suitable friction model as follows [33]:

$$f(\dot{q}) = f_{v_1}\dot{q} + f_{v_2}\text{sign}(\dot{q})\dot{q}^2 + f_c\text{sign}(\dot{q}) + f_o \quad (4)$$

where f_{v_1} and f_{v_2} represent the viscous friction coefficient, and f_c and f_o represent the Coulomb friction coefficient and the friction bias term, respectively.

Suppose that the robot's end-effector is devoid of any load over the process of dynamics identification, i.e., $\tau_d = 0$. Since the dynamic model of the robot manipulator is linear with respect to the dynamic parameters, based on the linearity property [6], system (1) can be transformed into the following linearized parameterized form:

$$\tau = Y_s(q, \dot{q}, \ddot{q})\beta_s \quad (5)$$

where $\mathbf{Y}_s(\mathbf{q}, \dot{\mathbf{q}}, \ddot{\mathbf{q}}) \in \mathbb{R}^{n \times s}$ and $\boldsymbol{\beta}_s \in \mathbb{R}^s$ denote the regressor function and the standard parameters, respectively, while s is the number of standard parameters. Notably, for each link, $\boldsymbol{\beta}_s$ consists of a total of 15 parameters, encompassing 10 link-related parameters— I_{xx_i} , I_{yy_i} , I_{zz_i} , I_{xy_i} , I_{xz_i} , I_{yz_i} as inertia parameters, m_i as joint mass, and l_{x_i} , l_{y_i} , l_{z_i} as first-order mass moments—and 5 motor-related parameters— J_i as moment of inertia and $f_{v_{1i}}$, $f_{v_{2i}}$, f_{c_i} , f_{o_i} as friction parameters, with the subscript i denoting the i -th link.

Nonetheless, $\mathbf{Y}_s(\mathbf{q}, \dot{\mathbf{q}}, \ddot{\mathbf{q}})$ encompasses a substantial number of zero columns and linearly dependent columns, rendering the matrix non-invertible. Thus, by reorganizing linearly independent columns [34], we can further formulate system (5) as the following simplified dynamic model:

$$\boldsymbol{\tau} = \mathbf{Y}_b(\mathbf{q}, \dot{\mathbf{q}}, \ddot{\mathbf{q}})\boldsymbol{\beta}_b \quad (6)$$

where $\mathbf{Y}_b(\mathbf{q}, \dot{\mathbf{q}}, \ddot{\mathbf{q}}) \in \mathbb{R}^{n \times r}$ and $\boldsymbol{\beta}_b \in \mathbb{R}^r$ represent the subset of the maximum linear independent columns of $\mathbf{Y}_s(\mathbf{q}, \dot{\mathbf{q}}, \ddot{\mathbf{q}})$ and the base parameters comprising a total of r elements, respectively.

Ultimately, the robot manipulator is executed along the excitation trajectory for N cycles, during which experimental data are collected as expressed by

$$\mathbf{T} = \mathbf{Y}\boldsymbol{\beta}_b \quad (7)$$

where $\mathbf{Y} = [\mathbf{Y}_{b_1}^\top, \mathbf{Y}_{b_2}^\top, \dots, \mathbf{Y}_{b_N}^\top]^\top$ and $\mathbf{T} = [\boldsymbol{\tau}_1^\top, \boldsymbol{\tau}_2^\top, \dots, \boldsymbol{\tau}_N^\top]^\top$. Consequently, the base parameters $\boldsymbol{\beta}_b$ can be determined by using the least squares estimation technique [35].

Up to this point, we have successfully established the dynamic model (6) of the robot manipulator, thereby laying the foundation for forthcoming endeavors in disturbance observer and controller design. Furthermore, explicit formulations for $\mathbf{M}(\mathbf{q})$, $\mathbf{C}(\mathbf{q}, \dot{\mathbf{q}})$, $\mathbf{G}(\mathbf{q})$, and $\mathbf{f}(\dot{\mathbf{q}})$ can be readily derived through straightforward algebraic manipulations [32].

3.2. Uncertain Dynamics Estimation

In the preceding section, we assume that $\boldsymbol{\tau}_d = 0$. However, in real-world scenarios, particularly during the operation of the robot manipulator, the value of $\boldsymbol{\tau}_d$ cannot be disregarded. As a result, in this section, we will proceed to develop a STDO aimed at providing a precise estimation of $\mathbf{d}(t)$.

Firstly, by extending $\mathbf{d}(t)$ as a new state vector \mathbf{x}_3 , system (2) can be reformulated as

$$\begin{cases} \dot{\mathbf{x}}_2 = \mathbf{u} + \mathbf{F}(\mathbf{x}_1, \mathbf{x}_2) + \mathbf{x}_3 \\ \dot{\mathbf{x}}_3 = \dot{\mathbf{d}}(t). \end{cases} \quad (8)$$

For system (8), the following STDO is designed:

$$\begin{cases} \dot{\hat{\mathbf{x}}}_2 = \mathbf{u} + \mathbf{F}(\mathbf{x}_1, \mathbf{x}_2) + \hat{\mathbf{x}}_3 + \kappa_1 \text{sig}^{1/2}(\mathbf{x}_2 - \hat{\mathbf{x}}_2) \\ \dot{\hat{\mathbf{x}}}_3 = \kappa_2 \text{sign}(\mathbf{x}_2 - \hat{\mathbf{x}}_2) \end{cases} \quad (9)$$

where $\hat{\mathbf{x}}_2, \hat{\mathbf{x}}_3$ are the estimates of $\mathbf{x}_2, \mathbf{x}_3$, respectively, and $\kappa_1, \kappa_2 \in \mathbb{R}^{n \times n}$ are the observer parameters, both of which are the positive definite diagonal matrices to be designed.

Let $e_1 = \mathbf{x}_2 - \hat{\mathbf{x}}_2$, $e_2 = \mathbf{x}_3 - \hat{\mathbf{x}}_3$ be the observation errors. By combining systems (8) and (9), the error equation of the disturbance observer can be obtained as

$$\begin{cases} \dot{e}_1 = e_2 - \kappa_1 \text{sig}^{1/2}(e_1) \\ \dot{e}_2 = -\kappa_2 \text{sign}(e_2) + \dot{\mathbf{d}}(t). \end{cases} \quad (10)$$

Based on the finite-stability analysis presented in reference [36], and considering Assumption 1, it is evident that the selection of $\kappa_1 = 1.5L^{1/2}$ and $\kappa_2 = 1.1L$ will lead to finite-time stability for system (10). That is, there exists a finite time constant T_0 after which e_1 and e_2 will converge to zero when time $t > T_0$.

3.3. Composite Position Predictive Control Design

Building upon the foundation of the offline identification model and estimations of unknown dynamics, this subsection primarily delves into the construction of a composite position predictive controller. The process is principally divided into three key steps.

3.3.1. State Transformation

First of all, following Assumption 2, the ensuing steady-state reference signal is established as follows:

$$\mathbf{x}_1^* = \mathbf{q}_d, \mathbf{x}_2^* = \dot{\mathbf{q}}_d, \mathbf{x}_3^* = \ddot{\mathbf{q}}_d - F(\mathbf{x}_1^*, \mathbf{x}_2^*) - \hat{\mathbf{x}}_3. \quad (11)$$

Next, perform the following coordinate transformation:

$$\boldsymbol{\eta}_1 = \mathbf{x}_1 - \mathbf{x}_1^*, \boldsymbol{\eta}_2 = \mathbf{x}_2 - \mathbf{x}_2^*, \mathbf{v} = \mathbf{u} - \mathbf{x}_3^* \quad (12)$$

Define a new state vector $\boldsymbol{\eta} = [\boldsymbol{\eta}_1^\top, \boldsymbol{\eta}_2^\top]^\top \in \mathbb{R}^{2n}$. Subsequently, concerning (11) and (12), system (2) can be reorganized as

$$\dot{\boldsymbol{\eta}} = \mathbf{A}\boldsymbol{\eta} + \mathbf{B}(\mathbf{v} + \mathbf{e}_2 + F(\mathbf{x}_1, \mathbf{x}_2) - F(\mathbf{x}_1^*, \mathbf{x}_2^*)) \quad (13)$$

where

$$\begin{aligned} \mathbf{A} &= \begin{bmatrix} \mathbf{0} \in \mathbb{R}^{n \times n} & \mathbf{I}_n \in \mathbb{R}^{n \times n} \\ \mathbf{0} \in \mathbb{R}^{n \times n} & \mathbf{0} \in \mathbb{R}^{n \times n} \end{bmatrix} \in \mathbb{R}^{2n \times 2n}, \\ \mathbf{B} &= \begin{bmatrix} \mathbf{0} \in \mathbb{R}^{n \times n} & \mathbf{I}_n \in \mathbb{R}^{n \times n} \end{bmatrix}^\top \in \mathbb{R}^{2n \times n}. \end{aligned}$$

System (13) will serve as the model foundation for the subsequent design of the composite position predictive controller.

3.3.2. Receding Optimization

To make the joint angle converge to its reference value at an optimal rate, the optimization performance index is selected as

$$J(t) = \frac{1}{2} \int_0^{T_p} \boldsymbol{\eta}_1^\top(t + \xi) \cdot \boldsymbol{\eta}_1(t + \xi) d\xi \quad (14)$$

where $T_p \in (0, 1)$ is the prediction horizon.

Subsequently, by disregarding the estimation error and the nonlinear tracking error term in system (13), we derive the nominal model as follows:

$$\dot{\boldsymbol{\eta}} = \mathbf{A}\boldsymbol{\eta} + \mathbf{B}\mathbf{v}. \quad (15)$$

Regarding the tracking error $\boldsymbol{\eta}_1$, the approximation within a single prediction cycle $[0, T_p]$, obtained through the application of a Taylor series expansion on the nominal model (15), leads to the following formula:

$$\begin{aligned} \hat{\boldsymbol{\eta}}_1(t + \xi) &= \boldsymbol{\eta}_1 + \xi \boldsymbol{\eta}_2 + \frac{\xi^2}{2} \mathbf{v} + \dots + \frac{\xi^{2+r}}{(2+r)!} \mathbf{v}^{(r)} \\ &= \mathbf{G}\boldsymbol{\eta} + \mathbf{H}\mathbf{v} \end{aligned} \quad (16)$$

where r is the control order of the system,

$$\begin{aligned}\mathbf{G} &= [\mathbf{I}_n \in \mathbb{R}^{n \times n}, \xi \mathbf{I}_n \in \mathbb{R}^{n \times n}] \in \mathbb{R}^{n \times 2n}, \\ \mathbf{H} &= \left[\frac{\xi^2}{2} \mathbf{I}_n, \frac{\xi^3}{3!} \mathbf{I}_n, \dots, \frac{\xi^{2+r}}{(2+r)!} \mathbf{I}_n \right] \in \mathbb{R}^{n \times n(r+1)}, \\ \mathbf{V} &= \left[\mathbf{v}^\top, \dot{\mathbf{v}}^\top, \dots, (\mathbf{v}^{(r)})^\top \right]^\top \in \mathbb{R}^{n(r+1) \times 1}.\end{aligned}$$

By substituting (16) into (14), the performance index defined in (14) can be further calculated as follows:

$$\begin{aligned}\hat{J}(t) &= \frac{1}{2} \int_0^{T_p} \hat{\eta}_1^\top(t + \xi) \cdot \hat{\eta}_1(t + \xi) d\xi \\ &= \frac{1}{2} \boldsymbol{\eta}^\top \mathbf{Q}_1 \boldsymbol{\eta} + \boldsymbol{\eta}^\top \mathbf{Q}_2 \mathbf{V} + \frac{1}{2} \mathbf{V}^\top \mathbf{Q}_3 \mathbf{V}\end{aligned}\quad (17)$$

where

$$\begin{aligned}\mathbf{Q}_1 &= \int_0^{T_p} \mathbf{G}^\top \mathbf{G} d\xi \in \mathbb{R}^{2n \times 2n}, \\ \mathbf{Q}_2 &= \int_0^{T_p} \mathbf{G}^\top \mathbf{H} d\xi \in \mathbb{R}^{2n \times n(r+1)}, \\ \mathbf{Q}_3 &= \int_0^{T_p} \mathbf{H}^\top \mathbf{H} d\xi \in \mathbb{R}^{n(r+1) \times n(r+1)}.\end{aligned}$$

Taking the partial derivative of $\hat{J}(t)$ with respect to \mathbf{V} yields $\partial \hat{J} / \partial \mathbf{V} = \boldsymbol{\eta}^\top \mathbf{Q}_2 + \mathbf{V}^\top \mathbf{Q}_3$. To obtain the optimal control vector \mathbf{V}^* , by setting $\partial \hat{J} / \partial \mathbf{V} = 0$, we can obtain

$$\mathbf{V}^* = -\mathbf{Q}_3^{-1} \mathbf{Q}_2^\top \boldsymbol{\eta}. \quad (18)$$

Following the principles of model predictive control theory, it is customary to designate the first column as the optimal control law. Consequently, the optimal control law can be further derived as

$$\mathbf{v}^* = -\mathbf{E} \mathbf{Q}_3^{-1} \mathbf{Q}_2^\top \boldsymbol{\eta} \quad (19)$$

where $\mathbf{E} = [\mathbf{I}_n, \mathbf{0}, \dots, \mathbf{0}] \in \mathbb{R}^{n \times n(r+1)}$.

3.3.3. Controller Implementation

For the ease of implementation in the controller algorithm, we choose the control order $r = 0$, therefore the optimization control law can be further calculated as

$$\mathbf{v} = \mathbf{v}^* \Big|_{r=0} = -\frac{\mathbf{K}_1^*}{T_p^2} \boldsymbol{\eta}_1 - \frac{\mathbf{K}_2^*}{T_p} \boldsymbol{\eta}_2 \quad (20)$$

where $\mathbf{K}_1^*, \mathbf{K}_2^* \in \mathbb{R}^n$ are constant diagonal matrices related to \mathbf{Q}_2 and \mathbf{Q}_3 .

Finally, combining (3), (11), and (12), we can get the composite PPC strategy as

$$\begin{aligned}\boldsymbol{\tau} &= \mathbf{M}(\mathbf{x}_1) \left(-\frac{\mathbf{K}_1^*}{T_p^2} \boldsymbol{\eta}_1 - \frac{\mathbf{K}_2^*}{T_p} \boldsymbol{\eta}_2 + \ddot{\mathbf{q}}_d - \mathbf{F}(\mathbf{x}_1^*, \mathbf{x}_2^*) - \hat{\mathbf{x}}_3 \right) \\ &= \mathbf{M}(\mathbf{q}) \left(\frac{\mathbf{K}_1^*}{T_p^2} (\mathbf{q}_d - \mathbf{q}) + \frac{\mathbf{K}_2^*}{T_p} (\dot{\mathbf{q}}_d - \dot{\mathbf{q}}) \right) \\ &\quad + \mathbf{C}(\mathbf{q}_d, \dot{\mathbf{q}}_d) \ddot{\mathbf{q}}_d + \mathbf{G}(\mathbf{q}_d) + \mathbf{f}(\dot{\mathbf{q}}_d) + \mathbf{M}(\mathbf{q})(\ddot{\mathbf{q}}_d - \hat{\mathbf{d}}).\end{aligned}\quad (21)$$

It can be observed from the controller (21) that the resulting optimized control law comprises the state feedback term, the dynamics feedforward term, and the observed

disturbance value. Furthermore, only the prediction horizon T_p needs adjustment, which significantly reduces the complexity of parameter tuning.

The comprehensive control block diagram is depicted in Figure 1.

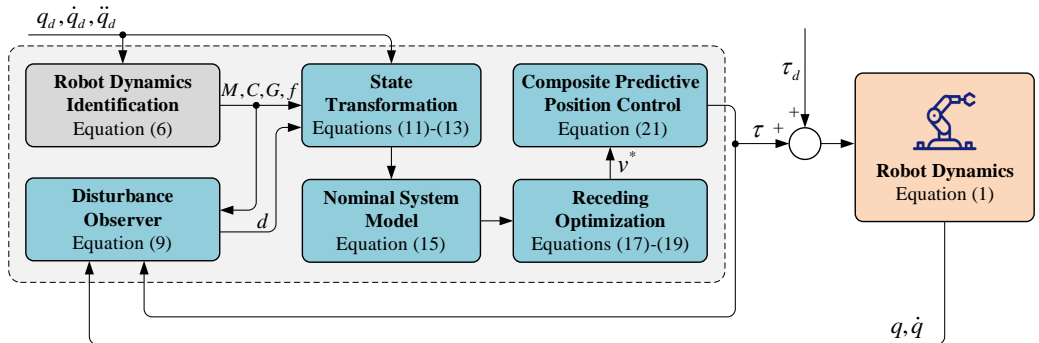


Figure 1. Control block diagram of the proposed control approach.

Remark 2. Typically, the traditional IDC is often linked with a proportional–integral–derivative (PID) type feedback control law, often formulated as follows:

$$\tau = M(\mathbf{q}) \left(K_p(\mathbf{q}_d - \mathbf{q}) + K_i \int_0^t (\mathbf{q}_d - \mathbf{q}) d\tau + K_d(\dot{\mathbf{q}}_d - \dot{\mathbf{q}}) \right) + C(\mathbf{q}, \dot{\mathbf{q}})\dot{\mathbf{q}} + G(\mathbf{q}) + f(\dot{\mathbf{q}}) + M(\mathbf{q})\ddot{\mathbf{q}}_d \quad (22)$$

where K_p , K_i , and K_d are the positive diagonal matrices to be designed. It is worth noting that this control approach heavily depends on precise robot dynamics. When an uncertain load is affixed to the robot's end-effector, it inevitably impacts positioning accuracy.

To tackle this challenge, a robust IDC can be developed by incorporating a nonlinear disturbance observer (NDO), which is designed as follows:

$$\tau = M(\mathbf{q}) (K_p(\mathbf{q}_d - \mathbf{q}) + K_d(\dot{\mathbf{q}}_d - \dot{\mathbf{q}})) + C(\mathbf{q}, \dot{\mathbf{q}})\dot{\mathbf{q}} + G(\mathbf{q}) + f(\dot{\mathbf{q}}) + M(\mathbf{q})(\ddot{\mathbf{q}}_d - \hat{\mathbf{d}}) \quad (23)$$

where the NDO is constructed as

$$\begin{cases} \hat{\mathbf{d}} = L_d(x_2 - p), \\ \dot{\mathbf{p}} = \mathbf{u} + F(x_1, x_2) + \hat{\mathbf{d}} \end{cases} \quad (24)$$

with L_d being the diagonal matrix to be designed.

However, when compared to the proposed controller (21), the composite IDC+NDO method exhibits the following drawbacks. It is well-established that utilizing NDO for the estimation of constant or slow time-varying disturbances proves to be effective. However, within robotic systems, the interactive coupling of various axes often leads to disturbances that are inherently nonlinear and time-varying. As a result, a certain degree of error unavoidably arises between the estimations and the actual values. To address this issue, we introduce the STDO, which is capable of achieving offset-free disturbance estimation within a finite time. This improvement significantly strengthens both the robustness and precision of robotic manipulation.

3.4. Stability Analysis

This section aims to provide a proof of the stability analysis of the closed-loop system.

Theorem 1. For an n -link robot manipulator described by the system dynamics (1), under the composite PPC approach combining the disturbance observer (9) and the optimal control action (21), with the proper selection of prediction horizon T_p , the tracking error η of the joint motion remains uniformly bounded, even in the presence of the external uncertain load.

Proof. To begin with, by introducing a coordinate transformation $\boldsymbol{\varepsilon}_i = T_p^{i-1} \boldsymbol{\eta}_i$, $i = 1, 2$, and further combining the system model (13), the transformed system associated with $\boldsymbol{\varepsilon}$ can be expressed by

$$\dot{\boldsymbol{\varepsilon}} = T_p^{-1}(\mathbf{A} - \mathbf{B}\mathbf{K})\boldsymbol{\varepsilon} + T_p(\mathbf{e}_2 + \tilde{\mathbf{F}}) \quad (25)$$

where $\boldsymbol{\varepsilon} = [\boldsymbol{\varepsilon}_1^\top, \boldsymbol{\varepsilon}_2^\top]^\top$, $\mathbf{K} = [\mathbf{K}_1^*, \mathbf{K}_2^*]$, $\tilde{\mathbf{F}} = \mathbf{F}(\mathbf{x}_1, \mathbf{x}_2) - \mathbf{F}(\mathbf{x}_1^*, \mathbf{x}_2^*)$. It is notable that, since $\mathbf{A} - \mathbf{B}\mathbf{K}$ is always Hurwitz stable, there exists a positive definite symmetric matrix $\mathbf{P} \in \mathbb{R}^{2n \times 2n}$ such that $(\mathbf{A} - \mathbf{B}\mathbf{K})^\top \mathbf{P} + \mathbf{P}(\mathbf{A} - \mathbf{B}\mathbf{K}) = -\mathbf{I}_{2n}$ is guaranteed.

Construct a Lyapunov function candidate as

$$V(\boldsymbol{\varepsilon}) = \boldsymbol{\varepsilon}^\top \mathbf{P} \boldsymbol{\varepsilon}. \quad (26)$$

By differentiating $V(\boldsymbol{\varepsilon})$ along the dynamics $\boldsymbol{\varepsilon}$ in (25), we obtain the following:

$$\begin{aligned} \dot{V}(\boldsymbol{\varepsilon}) &= \dot{\boldsymbol{\varepsilon}}^\top \mathbf{P} \boldsymbol{\varepsilon} + \boldsymbol{\varepsilon}^\top \mathbf{P} \dot{\boldsymbol{\varepsilon}} \\ &= \left(T_p^{-1}(\mathbf{A} - \mathbf{B}\mathbf{K})\boldsymbol{\varepsilon} + T_p(\mathbf{e}_2 + \tilde{\mathbf{F}}) \right)^\top \mathbf{P} \boldsymbol{\varepsilon} + \boldsymbol{\varepsilon}^\top \mathbf{P} \left(T_p^{-1}(\mathbf{A} - \mathbf{B}\mathbf{K})\boldsymbol{\varepsilon} + T_p(\mathbf{e}_2 + \tilde{\mathbf{F}}) \right) \\ &= T_p^{-1} \boldsymbol{\varepsilon}^\top (\mathbf{A} - \mathbf{B}\mathbf{K})^\top \mathbf{P} \boldsymbol{\varepsilon} + T_p(\mathbf{e}_2 + \tilde{\mathbf{F}})^\top \mathbf{P} \boldsymbol{\varepsilon} + T_p^{-1} \boldsymbol{\varepsilon}^\top \mathbf{P}(\mathbf{A} - \mathbf{B}\mathbf{K})\boldsymbol{\varepsilon} + T_p \boldsymbol{\varepsilon}^\top \mathbf{P}(\mathbf{e}_2 + \tilde{\mathbf{F}}) \\ &= T_p^{-1} \boldsymbol{\varepsilon}^\top ((\mathbf{A} - \mathbf{B}\mathbf{K})^\top \mathbf{P} + \mathbf{P}(\mathbf{A} - \mathbf{B}\mathbf{K}))\boldsymbol{\varepsilon} + 2T_p \boldsymbol{\varepsilon}^\top \mathbf{P}(\mathbf{e}_2 + \tilde{\mathbf{F}}) \\ &= -T_p^{-1} \boldsymbol{\varepsilon}^\top \boldsymbol{\varepsilon} + 2T_p \boldsymbol{\varepsilon}^\top \mathbf{P} \mathbf{e}_2 + 2T_p \boldsymbol{\varepsilon}^\top \mathbf{P} \tilde{\mathbf{F}}. \end{aligned} \quad (27)$$

Considering that, under the STDO (9), the disturbance estimation error is bounded, there must exist a bounded constant Γ such that $\sup \|\mathbf{e}_2\| \leq \Gamma$. Then, the second term in (27) can be specifically computed as

$$\begin{aligned} 2T_p \boldsymbol{\varepsilon}^\top \mathbf{P} \mathbf{e}_2 &\leq 2 \boldsymbol{\varepsilon}^\top \mathbf{P} \mathbf{e}_2 \\ &\leq 2 \lambda_{\max}(\mathbf{P}) \|\boldsymbol{\varepsilon}\| \|\mathbf{e}_2\| \\ &\leq \lambda_{\max}(\mathbf{P})^2 \|\boldsymbol{\varepsilon}\|^2 + \|\mathbf{e}_2\|^2 \\ &\leq \iota_1 \|\boldsymbol{\varepsilon}\|^2 + \Gamma^2 \end{aligned} \quad (28)$$

where $\iota_1 = \lambda_{\max}(\mathbf{P})^2$ and $\lambda_{\max}(\mathbf{P})$ represent the maximum eigenvalue of matrix \mathbf{P} .

Meanwhile, according to reference [37], there must exist a constant $\gamma \geq 0$, such that

$$\begin{aligned} T_p \tilde{\mathbf{F}} &\leq T_p \gamma (\|\mathbf{x}_1 - \mathbf{x}_1^*\| + \|\mathbf{x}_2 - \mathbf{x}_2^*\|) \\ &= T_p \gamma (\|\boldsymbol{\eta}_1\| + \|\boldsymbol{\eta}_2\|) \\ &= T_p \gamma (\|\boldsymbol{\varepsilon}_1\| + \|T_p^{-1} \boldsymbol{\varepsilon}_2\|) \\ &\leq \gamma (\|\boldsymbol{\varepsilon}_1\| + \|\boldsymbol{\varepsilon}_2\|) \\ &\leq \sqrt{2} \gamma \|\boldsymbol{\varepsilon}\|. \end{aligned} \quad (29)$$

Therefore, the third term in (27) can be reduced to

$$\begin{aligned} 2T_p \boldsymbol{\varepsilon}^\top \mathbf{P} \tilde{\mathbf{F}} &\leq 2 \|\boldsymbol{\varepsilon}\| \|\mathbf{P}\| \|T_p \tilde{\mathbf{F}}\| \\ &\leq 2\sqrt{2} \gamma \|\boldsymbol{\varepsilon}\| \|\mathbf{P}\| \|\boldsymbol{\varepsilon}\| \\ &\leq 2\sqrt{2} \gamma \lambda_{\max}(\mathbf{P}) \|\boldsymbol{\varepsilon}\|^2 \\ &= \iota_2 \|\boldsymbol{\varepsilon}\|^2. \end{aligned} \quad (30)$$

where $\iota_2 = 2\sqrt{2} \gamma \lambda_{\max}(\mathbf{P})$.

Substituting (28) and (30) into (27) yields

$$\dot{V}(\boldsymbol{\varepsilon}) \leq -\left(\frac{1}{T_p} - \iota_1 - \iota_2\right) \|\boldsymbol{\varepsilon}\|^2 + \Gamma^2. \quad (31)$$

With (31) in mind, we can establish the criterion for selecting the prediction horizon T_p in the proposed PPC method, which should satisfy the following inequality:

$$0 < T_p \leq \frac{1}{\iota_1 + \iota_2 + 1}. \quad (32)$$

Combining (31) and (32), we can further obtain the following:

$$\dot{V}(\varepsilon) \leq -\|\varepsilon\|^2 + \Gamma^2 \leq -\delta V(\varepsilon) + \Gamma^2 \quad (33)$$

where $\delta = 1/\lambda_{\max}(P)$. Furthermore, the following formula will hold:

$$0 \leq V(\varepsilon) \leq \left(V(0) - \frac{\Gamma^2}{\delta} \right) e^{-\delta t} + \frac{\Gamma^2}{\delta}. \quad (34)$$

It can be concluded from (34) that $V(\varepsilon)$ is bounded and converges exponentially, indicating that ε is uniformly bounded. This completes the proof. \square

4. Experimental Results

To validate the efficacy of the proposed control method, this section conducts a series of practical handling experiments on a real-world six-DOF robot manipulator subjected to varying load conditions.

4.1. Experimental Setup

The experimental platform comprises three main components: a motion control unit, a permanent magnet synchronous motor (PMSM) servo drive unit, and the robot body structure, as illustrated in Figure 2. Specifically, the motion control unit is implemented using a Beckhoff controller equipped with a PLC environment, which utilizes EtherCAT bus communication for the real-time control of the servo drives. These servo drives operate in the cyclic synchronous torque (CST) mode, receiving real-time torque signals from the motion controller with a control cycle of 1.0 ms. Furthermore, the robot body structure encompasses a six-DOF robot manipulator capable of executing movements in both the joint space and Cartesian space.

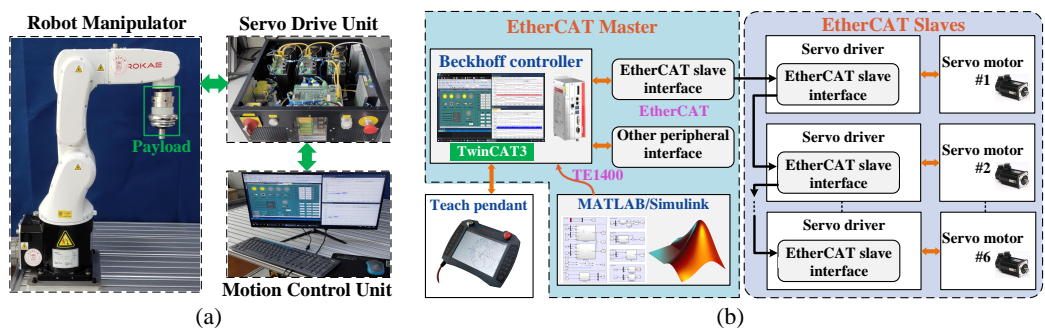


Figure 2. Experimental platform. (a) Hardware diagram. (b) System architecture.

As depicted in Figure 2b, the initial validation of the proposed control algorithm involved simulation in MATLAB/Simulink. We utilized the model-based design (MBD) methodology to create algorithm modules. Subsequently, the motion control unit was implemented in a Beckhoff controller, and the C++ files generated through MBD were imported using the TE1400 plugin. Finally, the algorithm modules were invoked and confirmed within the TwinCAT3 software (<https://www.beckhoff.com.cn/zh-cn/products/automation/twincat/>, accessed on 29 September 2023).

4.2. Dynamics Identification Results

The offline dynamics identification serves as the foundational step in implementing the proposed control method. This process begins by collecting real-time data related to the robot's trajectories, velocities, accelerations, and drive torques. Following this data collection, the dynamic base parameter set is determined through offline analysis utilizing the least squares method. The results of this experimental procedure are visualized in Figure 3.

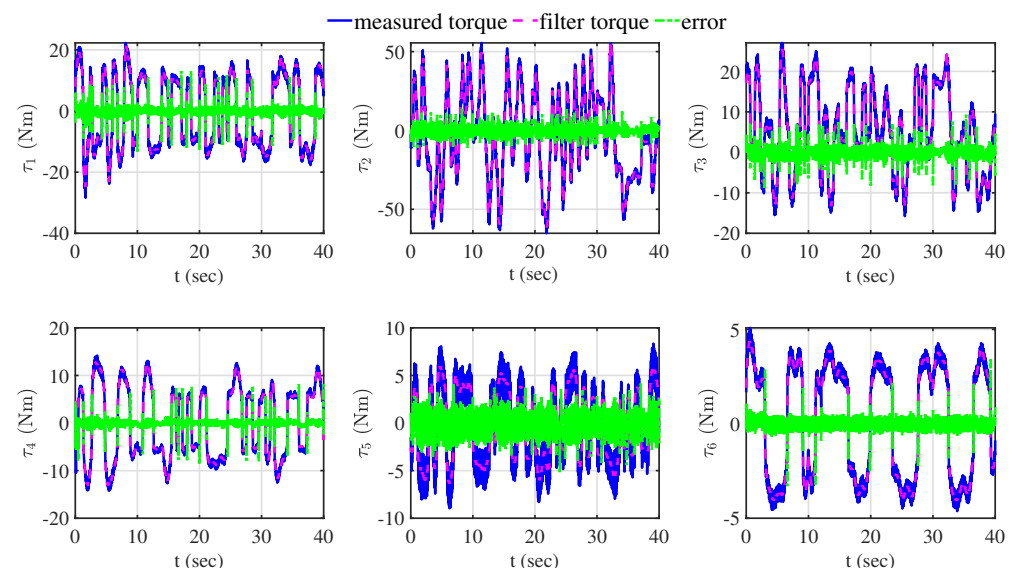


Figure 3. Dynamics identification results.

In these graphical representations, solid lines represent the actual torque measurements obtained during the execution of the excitation trajectories, whereas dashed lines depict the computed torques derived from the experimentally determined dynamic model. Notably, the errors (indicated by dotted lines) associated with the dynamic model consistently reside within a remarkably narrow range, which reveals that the identified dynamic model is relatively accurate.

4.3. Performance Validation

The feasibility and effectiveness of the proposed control strategy are further verified in terms of disturbance rejection capability and the steady-state control performance. To provide a basis for comparison, three distinct control strategies are devised: the traditional IDC method (22), the composite IDC+NDO method (23), and the proposed control method (PPC+STDO) (21).

4.3.1. Control Parameters Setting

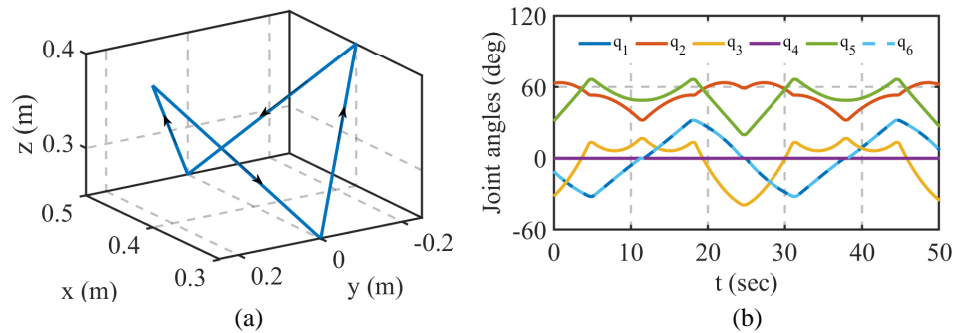
To ensure a fair comparison in the experiments, we maintained consistent test conditions and manually fine-tuned the parameters by using a trial-and-error approach for each controller. Then, we closely monitored the curves of control effort and fluctuations in tracking errors. As a general guideline, we expected the control effort to initially remain consistent. Furthermore, if the tracking errors remained largely unchanged while the fluctuations increased with larger parameter adjustments, it indicates that the parameters have been suitably selected. Finally, the parameter configurations for each controller are provided in Table 1.

Table 1. Parameters of three different controllers.

Controllers	Parameters
IDC	$K_p = \text{diag}\{6, 6, 6, 12, 12, 12\} \times 10^3$ $K_i = \text{diag}\{1.2, 1.2, 1.2, 1.5, 1.5, 1.5\} \times 10^4$ $K_d = \text{diag}\{25, 25, 25, 150, 150, 150\}$
IDC+NDO	$K_p = \text{diag}\{3.5, 3.5, 3.5, 10, 10, 10\} \times 10^3$ $K_d = \text{diag}\{25, 25, 25, 150, 150, 150\}$ $L_d = \text{diag}\{30, 30, 30, 30, 30, 30\}$
PPC+STDO	$K_1^* = \text{diag}\{3.3, 3.3, 3.3, 3.3, 3.3, 3.3\}$ $K_2^* = \text{diag}\{2.5, 2.5, 2.5, 2.5, 2.5, 2.5\}, T_p = 0.02$ $L = \text{diag}\{100, 100, 100, 100, 100, 100\}$

4.3.2. Trajectory Tracking Performance with Uncertain Load

To assess trajectory tracking performance, we conducted tracking experiments with 3D curves in Cartesian space under both light and heavy load conditions. Figure 4a illustrates the desired 3D curves, while Figure 4b displays the corresponding joint angles obtained using inverse kinematics.

**Figure 4.** Desired trajectories. (a) 3D desired trajectory. (b) Joint trajectories of the 3D curve.

Case 1: Executing a handling task under a light load condition.

In this case, an additional payload weighing 0.25 kg is affixed to the end-effector of the robot manipulator, as depicted in Figure 5a. The experimental results are presented in Figures 6–9.

**Figure 5.** End-effector load. (a) 0.7 kg. (b) 3.2 kg.

It is evident that the proposed PPC+STDO method offers distinct advantages when compared to the IDC and IDC+NDO approaches in terms of position tracking errors. Specifically, the proposed controller achieves minimal trajectory tracking errors, with each joint's maximum tracking error falling within a narrow range of 0.05 deg. In contrast, the traditional IDC method exhibits a maximum tracking error close to 0.25 deg. Figure 8 illustrates the disturbance estimation results of NDO and STDO, while Figure 9 represents the control inputs of these three methods. Notably, the comparison is fair because the control energy is within the same order of magnitude.

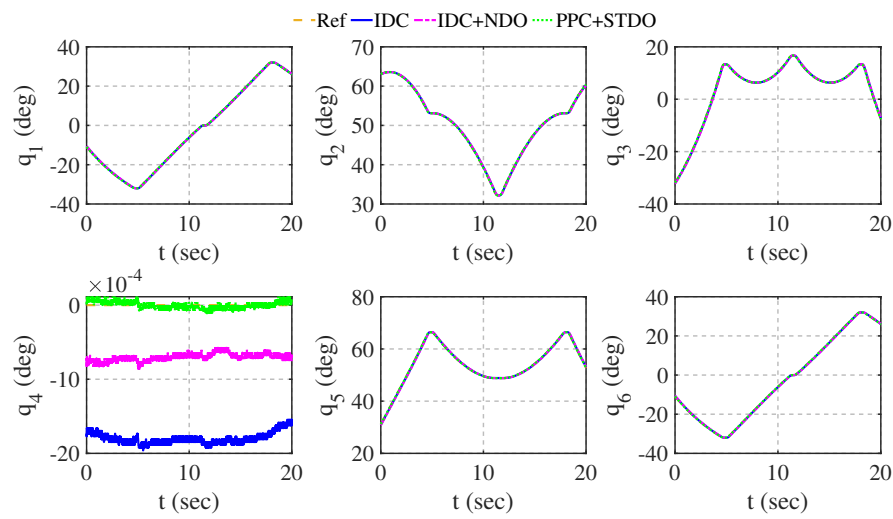


Figure 6. Trajectory tracking curves under Case 1.

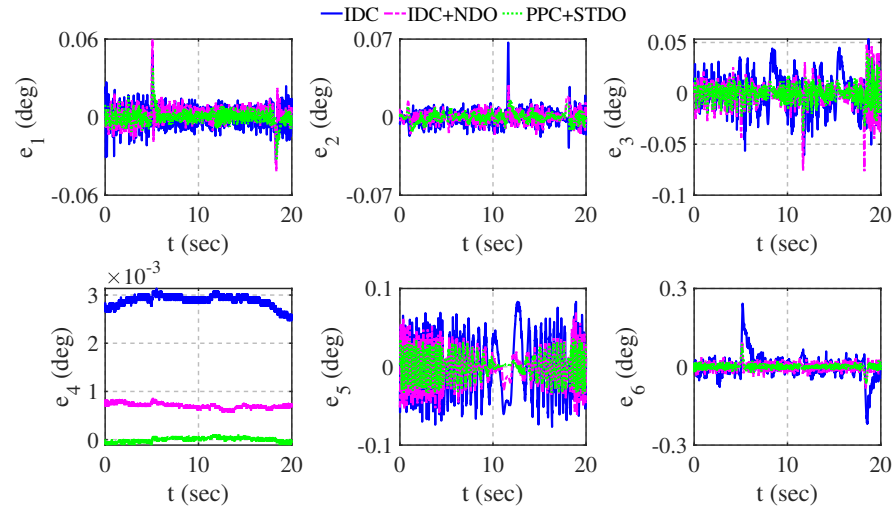


Figure 7. Trajectory tracking error curves under Case 1.

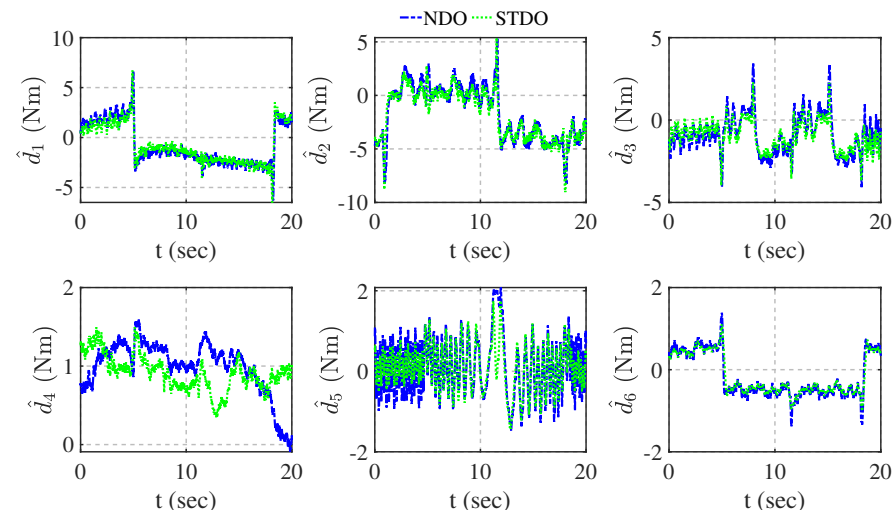


Figure 8. Disturbance estimation results under Case 1.

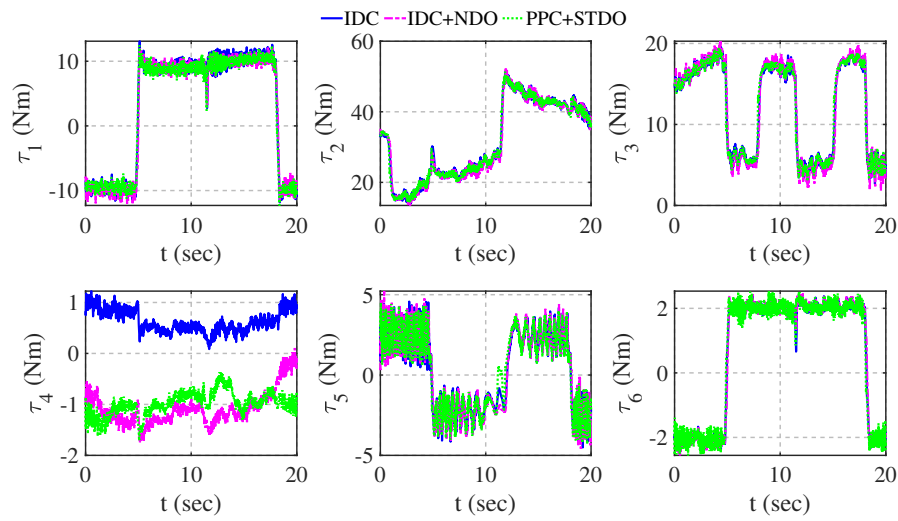


Figure 9. Control input curves under Case 1.

Case 2: Executing a handling task under a heavy load condition.

In this case, an additional payload weighing 3.2 kg is affixed to the end-effector of the robot manipulator, as depicted in Figure 5b. The experimental results are presented in Figures 10–13.

In contrast to Case 1, it is worth noting that Case 2 displays a higher level of system uncertainty. The experimental results clearly illustrate that the PPC+STDO method surpasses IDC+NDO and IDC in terms of disturbance rejection performance. Figure 12 presents the disturbance estimation results. Furthermore, as shown in Figure 9, it showcases smoother transitions in control energy and curve fluctuations compared to the other two control schemes. This can be attributed to the advantages facilitated by the offline dynamic identification provided by the proposed method.

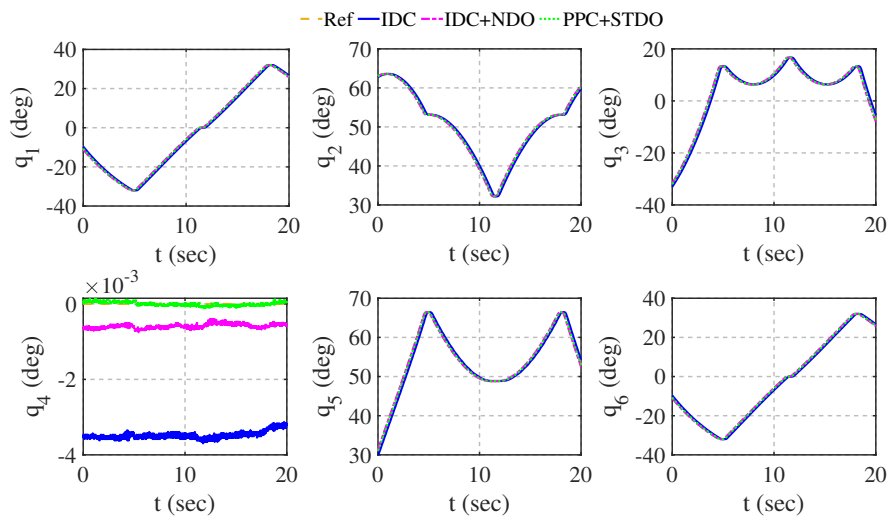


Figure 10. Trajectory tracking curves under Case 2.

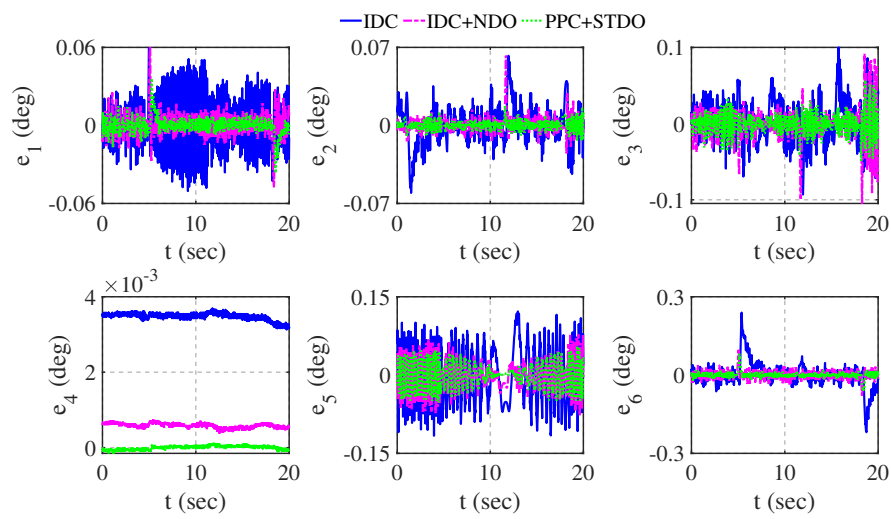


Figure 11. Trajectory tracking error curves under Case 2.

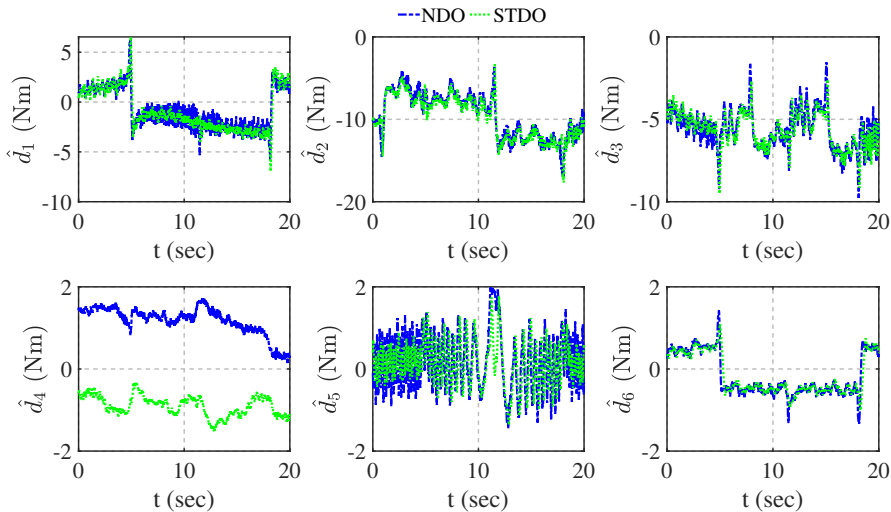


Figure 12. Disturbance estimation results under Case 2.

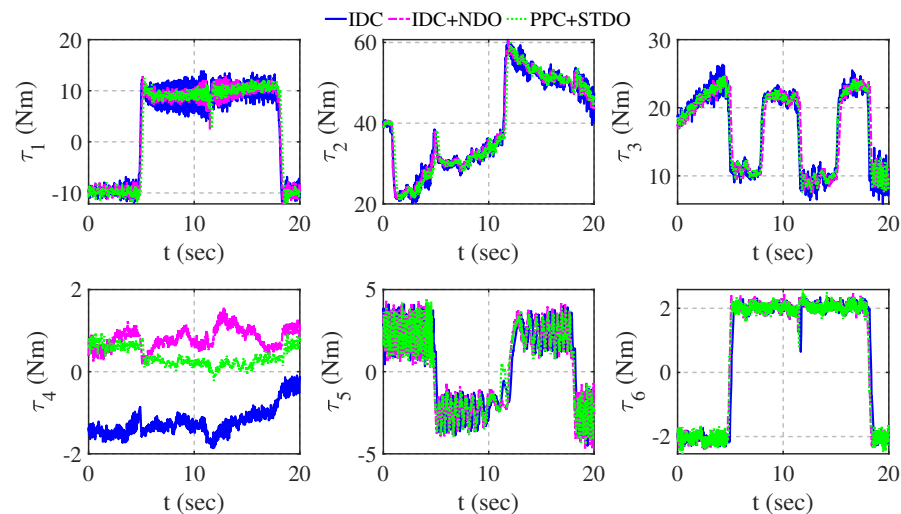


Figure 13. Control input curves under Case 2.

For a more intuitive analysis of the comparison, performance indices for all the control methods involved in two test cases are provided, which includes the root mean square error (RMSE) and the maximum absolute error (MAE), as shown in Table 2. The results indicate that the PPC+STDO method enhances tracking accuracy by approximately 45% and 25% when compared to the traditional IDC and the robust IDC+NDO approaches.

Table 2. Performance indices under different controllers.

Controllers	Joint 1 (deg)		Joint 2 (deg)		Joint 3 (deg)	
	RMSE	MAE	RMSE	MAE	RMSE	MAE
IDC	0.013	0.0104	0.013	0.0093	0.022	0.0178
IDC+NDO	0.008	0.0055	0.006	0.0041	0.019	0.0131
PPC+STDO	0.006	0.0037	0.005	0.0036	0.012	0.0086
Controllers	Joint 4 (deg)		Joint 5 (deg)		Joint 6 (deg)	
	RMSE	MAE	RMSE	MAE	RMSE	MAE
IDC	0.003	0.0032	0.046	0.040	0.043	0.026
IDC+NDO	6.5×10^{-4}	6.6×10^{-4}	0.025	0.020	0.015	0.0105
PPC+STDO	4.7×10^{-5}	4.0×10^{-5}	0.019	0.016	0.010	0.006

5. Conclusions

To enhance the trajectory tracking performance of robot manipulators, we have introduced a novel composite STDO-based PPC approach. The proposed control scheme has effectively integrated motion profile and disturbance preview elements into the dynamics and disturbance feedforward compensation. This comprehensive approach has significantly enhanced joint position tracking accuracy and bolstered robustness against disturbances, which is different from the conventional methods (e.g., IDC and IDC+NDO). We have validated the effectiveness of the proposed method using a real-world six-DOF robot manipulator. Comparative experiments have showcased the superior performance of our composite PPC approach in comparison to the conventional IDC methods. The results indicated that the proposed method can effectively solve the challenges related to accurate trajectory tracking and robust control in practical robot applications, which is also confirmed through quantitative analysis. In future work, we aim to address the challenge of state constraints within robot systems using the approach outlined in this paper.

Author Contributions: Conceptualization, S.R. and J.L.; methodology, S.R. and J.M.; software, S.R. and L.H.; validation, S.R. and J.M.; formal analysis, S.R. and L.H.; investigation, S.R.; data curation, S.R. and L.H.; writing—original draft preparation, S.R.; writing—review and editing, J.M. and J.L.; funding acquisition, J.M. All authors have read and agreed to the published version of the manuscript.

Funding: This work was funded in part by the National Natural Science Foundation of China under Grant 62203292, the National Key Research and Development Program of China under Grant 2021YFF0500904, and the Fundamental Research Funds for the Central Universities under Grant 2242022k30038.

Data Availability Statement: The data presented in this study are available on request from the corresponding author.

Acknowledgments: The authors express their sincere gratitude to the reviewers, associate editors, and editors for their invaluable feedback and dedicated time.

Conflicts of Interest: The authors declare no conflict of interest.

References

1. Alhama Blanco, P.J.; Abu-Dakka, F.J.; Abderrahim, M. Practical use of robot manipulators as intelligent manufacturing systems. *Sensors* **2018**, *18*, 2877. [[CrossRef](#)] [[PubMed](#)]
2. Hou, Y.; Li, J.; Chen, I.M. Self-supervised antipodal grasp learning with fine-grained grasp quality feedback in clutter. *IEEE Trans. Ind. Electron.* **2023**, *71*, 3853–3861. [[CrossRef](#)]

3. Li, Y.; Li, D.; Zhu, W.; Sun, J.; Zhang, X.; Li, S. Constrained motion planning of 7-DOF space manipulator via deep reinforcement learning combined with artificial potential field. *Aerospace* **2022**, *9*, 163. [[CrossRef](#)]
4. Drouot, A.; Zhao, R.; Irving, L.; Sanderson, D.; Ratchev, S. Measurement assisted assembly for high accuracy aerospace manufacturing. *IFAC-PapersOnLine* **2018**, *51*, 393–398. [[CrossRef](#)]
5. Mishchenko, Y.; Kaya, M.; Ozbay, E.; Yanar, H. Developing a three-to six-state EEG-based brain–computer interface for a virtual robotic manipulator control. *IEEE Trans. Biomed. Eng.* **2018**, *66*, 977–987. [[CrossRef](#)]
6. Spong, M.W.; Hutchinson, S.; Vidyasagar, M. *Robot Modeling and Control*; John Wiley & Sons: Hoboken, NJ, USA, 2020.
7. Xiao, B.; Yin, S. Exponential tracking control of robotic manipulators with uncertain dynamics and kinematics. *IEEE Trans. Ind. Inform.* **2018**, *15*, 689–698. [[CrossRef](#)]
8. Islam, S.; Liu, X.P. Robust sliding mode control for robot manipulators. *IEEE Trans. Ind. Electron.* **2010**, *58*, 2444–2453. [[CrossRef](#)]
9. Saied, H.; Chemori, A.; Bouri, M.; El Rafei, M.; Francis, C. Feedforward super-twisting sliding mode control for robotic manipulators: Application to PKMs. *IEEE Trans. Robot.* **2023**, *39*, 3167–3184. [[CrossRef](#)]
10. Dai, L.; Yu, Y.; Zhai, D.H.; Huang, T.; Xia, Y. Robust model predictive tracking control for robot manipulators with disturbances. *IEEE Trans. Ind. Electron.* **2020**, *68*, 4288–4297. [[CrossRef](#)]
11. Zhu, T.; Mao, J.; Han, L.; Zhang, C.; Yang, J. Real-time dynamic obstacle avoidance for robot manipulators based on cascaded nonlinear MPC with artificial potential field. *IEEE Trans. Ind. Electron.* **2023**, *early review*.
12. Wang, H. Adaptive control of robot manipulators with uncertain kinematics and dynamics. *IEEE Trans. Autom. Control* **2016**, *62*, 948–954. [[CrossRef](#)]
13. Jin, L.; Li, S.; Yu, J.; He, J. Robot manipulator control using neural networks: A survey. *Neurocomputing* **2018**, *285*, 23–34. [[CrossRef](#)]
14. He, W.; David, A.O.; Yin, Z.; Sun, C. Neural network control of a robotic manipulator with input deadzone and output constraint. *IEEE Trans. Syst. Man Cybern. Syst.* **2015**, *46*, 759–770. [[CrossRef](#)]
15. Yan, Y.; Wang, X.F.; Marshall, B.J.; Liu, C.; Yang, J.; Chen, W.H. Surviving disturbances: A predictive control framework with guaranteed safety. *Automatica* **2023**, *158*, 111238. [[CrossRef](#)]
16. DeHaan, D.; Guay, M. A real-time framework for model-predictive control of continuous-time nonlinear systems. *IEEE Trans. Autom. Control* **2007**, *52*, 2047–2057. [[CrossRef](#)]
17. Yang, J.; Zheng, W.X.; Li, S.; Wu, B.; Cheng, M. Design of a prediction-accuracy-enhanced continuous-time MPC for disturbed systems via a disturbance observer. *IEEE Trans. Ind. Electron.* **2015**, *62*, 5807–5816. [[CrossRef](#)]
18. Dong, X.; Mao, J.; Yan, Y.; Zhang, C.; Yang, J. Generalized dynamic predictive control for nonlinear systems subject to mismatched disturbances with application to PMSM drives. *IEEE Trans. Ind. Electron.* **2024**, *71*, 954–964. [[CrossRef](#)]
19. Zhang, C.; Li, M.; Zhou, L.; Cui, C.; Xu, L. A variable self-tuning horizon mechanism for generalized dynamic predictive control on DC/DC boost converters feeding CPLs. *IEEE J. Emerg. Sel. Top. Power Electron.* **2022**, *11*, 1650–1660. [[CrossRef](#)]
20. Li, S.; Yang, J.; Chen, W.H.; Chen, X. Generalized extended state observer based control for systems with mismatched uncertainties. *IEEE Trans. Ind. Electron.* **2011**, *59*, 4792–4802. [[CrossRef](#)]
21. Zhang, S.; Dong, Y.; Ouyang, Y.; Yin, Z.; Peng, K. Adaptive neural control for robotic manipulators with output constraints and uncertainties. *IEEE Trans. Neural Netw. Learn. Syst.* **2018**, *29*, 5554–5564. [[CrossRef](#)]
22. Mao, J.; Yang, J.; Liu, X.; Li, S.; Li, Q. Modeling and robust continuous TSM control for an inertially stabilized platform with couplings. *IEEE Trans. Control Syst. Technol.* **2019**, *28*, 2548–2555. [[CrossRef](#)]
23. Calafiore, G.C.; Fagiano, L. Robust model predictive control via scenario optimization. *IEEE Trans. Autom. Control* **2012**, *58*, 219–224. [[CrossRef](#)]
24. Chen, W.H.; Yang, J.; Guo, L.; Li, S. Disturbance-observer-based control and related methods—An overview. *IEEE Trans. Ind. Electron.* **2015**, *63*, 1083–1095. [[CrossRef](#)]
25. Nerkar, S.; Londhe, P.; Patre, B. Design of super twisting disturbance observer based control for autonomous underwater vehicle. *Int. J. Dyn. Control* **2022**, *10*, 306–322. [[CrossRef](#)]
26. Lei, M.; Wu, X.; Zhang, Y.; Ke, L. Super-twisting disturbance-observer-based nonlinear control of the overhead crane system. *Nonlinear Dyn.* **2023**, *111*, 14015–14025. [[CrossRef](#)]
27. Cui, L.; Hou, X.; Zuo, Z.; Yang, H. An adaptive fast super-twisting disturbance observer-based dual closed-loop attitude control with fixed-time convergence for UAV. *J. Frankl. Inst.* **2022**, *359*, 2514–2540. [[CrossRef](#)]
28. Mirzaei, M.; Asadollahi, M.; Aslmostafa, E.; Badamchizadeh, M. Continuous robust control based on fixed-time super-twisting disturbance observer. *IEEE Trans. Syst. Man Cybern. Syst.* **2023**, *early review*.
29. Pannocchia, G.; Bemporad, A. Combined design of disturbance model and observer for offset-free model predictive control. *IEEE Trans. Autom. Control* **2007**, *52*, 1048–1053. [[CrossRef](#)]
30. Xu, Q.; Yan, Y.; Zhang, C.; Dragicevic, T.; Blaabjerg, F. An offset-free composite model predictive control strategy for DC/DC buck converter feeding constant power loads. *IEEE Trans. Power Electron.* **2019**, *35*, 5331–5342. [[CrossRef](#)]
31. Li, M.; Lang, J.; Zhang, C.; Cui, C.; Xu, L. Decentralized composite generalized predictive control strategy for DC microgrids with high PV penetration. *Int. J. Robust Nonlinear Control* **2022**, *32*, 7793–7808. [[CrossRef](#)]
32. Han, L.; Mao, J.; Cao, P.; Gan, Y.; Li, S. Toward sensorless interaction force estimation for industrial robots using high-order finite-time observers. *IEEE Trans. Ind. Electron.* **2021**, *69*, 7275–7284. [[CrossRef](#)]

33. Wolf, S.; Iskandar, M. Extending a dynamic friction model with nonlinear viscous and thermal dependency for a motor and harmonic drive gear. In Proceedings of the 2018 IEEE International Conference on Robotics and Automation (ICRA), Brisbane, Australia, 21–25 May 2018; pp. 783–790.
34. Gautier, M.; Khalil, W. Direct calculation of minimum set of inertial parameters of serial robots. *IEEE Trans. Robot. Autom.* **1990**, *6*, 368–373. [[CrossRef](#)]
35. Jin, J.; Gans, N. Parameter identification for industrial robots with a fast and robust trajectory design approach. *Robot. Comput.-Integr. Manuf.* **2015**, *31*, 21–29. [[CrossRef](#)]
36. Moreno, J.A.; Osorio, M. Strict Lyapunov functions for the super-twisting algorithm. *IEEE Trans. Autom. Control* **2012**, *57*, 1035–1040. [[CrossRef](#)]
37. Zhang, C.; Yang, J.; Wen, C.; Wang, L.; Li, S. Realization of exact tracking control for nonlinear systems via a nonrecursive dynamic design. *IEEE Trans. Syst. Man Cybern. Syst.* **2017**, *50*, 577–589. [[CrossRef](#)]

Disclaimer/Publisher’s Note: The statements, opinions and data contained in all publications are solely those of the individual author(s) and contributor(s) and not of MDPI and/or the editor(s). MDPI and/or the editor(s) disclaim responsibility for any injury to people or property resulting from any ideas, methods, instructions or products referred to in the content.